Time-Delay Estimation using Ground Penetrating Radar with a Support Vector Regression based Linear Prediction Method

Jingjing Pan, Cédric Le Bastard, Yide Wang, Meng Sun

Time-Delay Estimation using Ground Penetrating Radar with a Support Vector Regression based Linear Prediction Method

Jingjing Pan, Cédric Le Bastard, Yide Wang, *Member, IEEE,* and Meng Sun

Abstract—**Ground penetrating radar (GPR) is widely used in media parameters estimation and targets localization. This paper focuses on time-delay estimation (TDE) using GPR signal, which contains important information about the probed media structure. But TDE tends to be a challenging task in GPR applications, in the scenarios of overlapping, coherent signals and limited snapshots. Forward-backward linear prediction (FBLP) is a high time resolution method, which is able to directly deal with coherent signals. Support vector regression (SVR) is robust with small samples. Therefore, we propose to combine the theory of FBLP and SVR together to enhance the robustness of TDE in the case of coherent, overlapping signals as well as limited snapshots. The proposed method is tested both with numerical and experimental data. Both of the results demonstrate the effectiveness of the proposed method.**

Index Terms—**Ground Penetrating Radar (GPR), Support Vector Regression (SVR), Forward-Backward Linear Prediction (FBLP), Time-Delay Estimation (TDE), low snapshots.**

I. INTRODUCTION

GROUND penetrating radar (GPR) is a common tool for subsurface sensing in the field of civil engineering, defense, agriculture and environment [1]–[3]. It allows non-destructive probing and therefore gains much interest both in media parameters estimation and in buried targets localization [4]–[6].

In civil engineering, GPR is used to survey horizontally stratified media, for example, roadways. The information of the vertical structure of the stratified media can be extracted from radar profiles by means of echo detection and amplitude estimation. Echo detection provides the time-delay estimation (TDE) associated with each interface, whereas amplitude estimation is used to retrieve the wave speed within each layer. However, TDE has several signal processing challenges in practical GPR applications. Problem arises when the backs-cattered echoes are too close to each other, which requires the use of signal processing algorithms with high temporal resolution. Subspace methods and linear prediction (LP) are

J. Pan and Y. Wang are with UMR CNRS 6164-Polytech Nantes, Institute of Electronics and Telecommunications of Rennes, Université de Nantes, Nantes 44306, France.

C. Le Bastard is with Project-team ENSUM, Centre for Studies and Expertise on Risks, Environment, Mobility, and Urban and Country Planning, 49136 Les Ponts de Cé, France, and also researcher associated with the UMR CNRS 6164Polytech Nantes, Institute of Electronics and Telecommunications of Rennes, Université de Nantes, Nantes 44306, France.

M. Sun is with Information Engineering College, Shanghai Maritime University, Shanghai 201306, China. (E-mail: msun@shmtu.edu.cn)

Manuscript received March 27 2017;

more appropriate than the conventional FFT-based methods for estimating time-delays of overlapping echoes [2]. Furthermore, the performance of signal processing algorithms degrades when the number of available snapshots used for covariance matrix estimation is limited [7]–[9]. In addition, the backscattered echoes obtained from GPR are usually highly correlated (even coherent) with each other, which significantly adds up to the difficulties in TDE. Decorrelation techniques [5], [10], [11] are attractive, especially with subspace methods, like multiple signal classification (MUSIC) [12] and estimation of signal parameters via rational invariance technique (ESPRIT) [13].

It is worth noting that LP methods have a high temporal resolution. They are able to perform spatial smoothing implicitly [10], which is of great importance with coherent signals. In GPR applications, there has been a considerable number of research making use of LP in the detection of buried objects [8], [14]–[16]. LP is used to predict the next GPR signal from the previous observations. An object appears when the measured signal is different from the prediction. There are also applications about autoregressive model (AR, one-side LP) in the estimation of parameters of subsurface materials, for example, the estimation of time-delay [2] and soil permittivity [17]. Nevertheless, the performance of LP is limited when the observation records are short [8].

In essence, LP methods are about the estimation of a weight vector. A promising solution to the estimation problem due to the short observation records is the support vector regression (SVR) [18]. SVR is the regression form of support vector machine (SVM). Based on the principle of structural risk minimization, SVR has fantastic generalization ability. It is originally used only in the real domain and later extended into complex form [7], [19], [20]. In the literature, SVR has been integrated with several linear signal processing algorithms. A support vector autoregressive method (AR-SVR) is proposed for frequency estimation problems [21], [22]. The authors in [23] combines autoregressive moving average (ARMA) with SVR for system identification applications. The theory of AR is closely related to the forward linear prediction (FLP) [24]. However, forward-backward linear prediction (FBLP) performs better than one-side prediction methods (FLP and backward linear prediction, BLP) [25]. Therefore, we propose to combine the theory of SVR with FBLP together in TDE. The objective function can be transformed from complex to real domain like in [7]. In this paper, the function is directly formulated in complex domain with Wirtinger's calculus [20], [26].

The remainder of the paper is organized as follows. Section II presents the signal model. Section III introduces the theory of FBLP and the proposed SVR based FBLP method. Section IV presents some simulation results. Section V shows the performance of the proposed method with experimental data. The conclusion is drawn in Section VI.

In the following, $(.)^T$, $(.)^*$, and $(.)^H$ denote transpose, conjugate, and complex conjugate transpose operations, respectively. $\mathbb{R}$ and $\mathbb{C}$ denote real and complex sets, respectively. $Re(\mathbf{z})$ and $Im(\mathbf{z})$ denote the real and imaginary parts of $\mathbf{z}$, respectively. Vectors and matrices appear in boldface lowercase letters and boldface capital letters, respectively.

II. SIGNAL MODEL

The signal model used in [2], [11], [27] with stratified media is adopted in this paper. Thus, the backscattered echoes are the time-shifted and attenuated replicas of the transmitted signal. The observation is performed with M discrete frequencies. The frequency f_m is defined as $f_m = f_1 + (m-1)\Delta f$, with f_1 the beginning of the bandwidth and Δf the frequency shift, $m = 1, \ldots, M$. The received signal at frequency f_m can be expressed in frequency domain as

$$g(f_m) = \sum_{k=1}^{K} e(f_m)s_k e^{-j2\pi f_m \tau_k} + n(f_m) \qquad (1)$$

where K is the number of backscattered echoes, which can be primary and multiple reflection echoes. s_k denotes the amplitude of the kth backscattered echo. τ_k is the kth time-delay corresponding to the kth echo. At frequency f_m, $e(f_m)$ represents the radar pulse in frequency domain while $n(f_m)$ is an additive white Gaussian noise with zero mean and variance σ^2.

In order to use the principle of LP methods, a whitening procedure [2], [5] is applied. In the following, each echo is divided by the radar pulse. Thus, (1) becomes:

$$r_m = \frac{g(f_m)}{e(f_m)} = \sum_{k=1}^{K} s_k e^{-j2\pi f_m \tau_k} + \frac{n(f_m)}{e(f_m)}. \qquad (2)$$

With L independent snapshots, the data sample at frequency f_m can be written as

$$\mathbf{r}_m = [r_m(1), r_m(2), \ldots, r_m(L)]^T. \qquad (3)$$

III. METHODOLOGY

A. Forward-backward linear prediction

In theory, LP estimates the unknown samples with a linear combination of the known observations by minimizing the mean square prediction error. FBLP uses the observations from both forward and backward observation sequences. If the order of the prediction filter equals P, the prediction equation can be modeled as [28], [29]:

$$\begin{bmatrix} \mathbf{r}_P & \mathbf{r}_{P-1} & \cdots & \mathbf{r}_1 \\ \vdots & \vdots & & \vdots \\ \mathbf{r}_{M-1} & \mathbf{r}_{M-2} & \cdots & \mathbf{r}_{M-P} \\ \cdots\cdots\cdots\cdots\cdots\cdots\cdots\cdots\cdots \\ \mathbf{r}_2^* & \mathbf{r}_3^* & \cdots & \mathbf{r}_{P+1}^* \\ \vdots & \vdots & \vdots & \\ \mathbf{r}_{M-P+1}^* & \mathbf{r}_{M-P+2}^* & \cdots & \mathbf{r}_M^* \end{bmatrix} \begin{bmatrix} \omega_1 \\ \vdots \\ \omega_P \end{bmatrix} = \begin{bmatrix} \mathbf{r}_{P+1} \\ \vdots \\ \mathbf{r}_M \\ \cdots\cdots \\ \mathbf{r}_1^* \\ \vdots \\ \mathbf{r}_{M-P}^* \end{bmatrix}. \qquad (4)$$

The other LP methods, FLP or BLP, can be expressed with the first or second half (above or below dotted line) of (4), respectively. In a more compact way, (4) can be written as

$$\mathbf{X}\boldsymbol{\omega} = \mathbf{y} \qquad (5)$$

where $\mathbf{y} \in \mathbb{C}^{N_T \times 1}$, $\mathbf{X} \in \mathbb{C}^{N_T \times P}$ and $\boldsymbol{\omega} \in \mathbb{C}^{P \times 1}$, $N_T = 2(M-P)L$.

The weight coefficient vector $\boldsymbol{\omega}$ can be estimated by [28]:

$$\boldsymbol{\omega} = \mathbf{R}^{-1}\mathbf{r} \qquad (6)$$

where $\mathbf{R} = \mathbf{X}^H\mathbf{X}/L$ and $\mathbf{r} = \mathbf{X}^H\mathbf{y}/L$. The inversion of $\mathbf{R}$ requires the inequality constraint: $N_T \geqslant P$. Therefore, we have the constraint on the number of snapshots L, $L \geq P/[2(M-P)]$.

The order of the prediction filter P should satisfy: $K \leqslant P \leqslant M - K/2$ [29].

The time-delay of each echo can be estimated by searching the peak positions in the power spectrum density (PSD) of FBLP. With the weight vector $\boldsymbol{\omega}$, the PSD is defined as

$$P(t) = \frac{1}{\left| \boldsymbol{a}^H(t) \begin{bmatrix} 1 \\ -\boldsymbol{\omega} \end{bmatrix} \right|^2} \qquad (7)$$

with $\boldsymbol{a}(t) = [e^{-2j\pi f_1 t}, e^{-2j\pi f_2 t}, \ldots, e^{-2j\pi f_{P+1} t}]^T$, the mode vector.

B. Proposed method: FBLP-SVR

The key issue in LP methods is to estimate the weight vector $\boldsymbol{\omega}$. However, in scenarios where the number of available snapshots is insufficient, the performance of LP methods suffers great deterioration. The principle of SVR works not only with limited number of samples but also with complex data. Therefore, we propose to combine SVR with FBLP in this paper, which is called FBLP-SVR in the following.

We can see that (5) is a typical form of SVR in complex domain. In this paper, SVR is directly formulated in complex domain to deal with complex data in a natural way [19], [20]. The research in [20] deals with complex-valued nonlinear regression problems by exploiting the widely linear estimation method in complex domain, which is very instructive in finding the solution of (5). In regression problems, the main objective of SVR is to find a hyper plane to fit the data within a deviation less than a given value ϵ. The ϵ-insensitive loss function is used here [30]. The primal objective function is to minimize the prediction error both structurally and empirically. Since the

empirical errors are complex-valued, the residuals should be minimized both in their real and imaginary parts. Therefore, the optimization task can be expressed as [19], [20], [30]:

$$\min_{\boldsymbol{\omega},\boldsymbol{\xi}^r,\hat{\boldsymbol{\xi}}^r,\boldsymbol{\xi}^i,\hat{\boldsymbol{\xi}}^i} (\frac{1}{2}\|\boldsymbol{\omega}\|^2 + C\sum_{n=1}^{N_T}(\xi_n^r + \hat{\xi}_n^r + \xi_n^i + \hat{\xi}_n^i)) \quad (8)$$

$$\text{s. t.} \begin{cases} Re(y_n - \mathbf{x}_n^H\boldsymbol{\omega}) \leqslant \epsilon + \xi_n^r, n = 1,\ldots,N_T \\ Re(-y_n + \mathbf{x}_n^H\boldsymbol{\omega}) \leqslant \epsilon + \hat{\xi}_n^r, n = 1,\ldots,N_T \\ Im(y_n - \mathbf{x}_n^H\boldsymbol{\omega}) \leqslant \epsilon + \xi_n^i, n = 1,\ldots,N_T \\ Im(-y_n + \mathbf{x}_n^H\boldsymbol{\omega}) \leqslant \epsilon + \hat{\xi}_n^i, n = 1,\ldots,N_T \\ \xi_n^r, \hat{\xi}_n^r, \xi_n^i, \hat{\xi}_n^i \geqslant 0, n = 1,\ldots,N_T \end{cases}$$

where $\mathbf{x}_n$ is the nth column of $\mathbf{X}^H$ and $y_n = \mathbf{y}(n)$, $n = 1,\ldots,N_T$. ξ_n^r and $\hat{\xi}_n^r$ stand for positive and negative errors in the real part of y_n while ξ_n^i and $\hat{\xi}_n^i$ are for the corresponding imaginary part. The value C controls the trade-off between the structural and empirical errors.

The method of Lagrangian multipliers is employed to find the solutions of (8) by introducing a dual set variables. Therefore, we have the primal-dual objective function:

$$L_{pd}(\boldsymbol{\omega}) = \frac{1}{2}\|\boldsymbol{\omega}\|^2 + C\sum_{n=1}^{N_T}(\xi_n^r + \hat{\xi}_n^r + \xi_n^i + \hat{\xi}_n^i)$$
$$+ \sum_{n=1}^{N_T} a_n(Re(y_n - \mathbf{x}_n^H\boldsymbol{\omega}) - \epsilon - \xi_n^r)$$
$$+ \sum_{n=1}^{N_T} \hat{a}_n(Re(-y_n + \mathbf{x}_n^H\boldsymbol{\omega}) - \epsilon - \hat{\xi}_n^r)$$
$$+ \sum_{n=1}^{N_T} b_n(Im(y_n - \mathbf{x}_n^H\boldsymbol{\omega}) - \epsilon - \xi_n^i)$$
$$+ \sum_{n=1}^{N_T} \hat{b}_n(Im(-y_n + \mathbf{x}_n^H\boldsymbol{\omega}) - \epsilon - \hat{\xi}_n^i)$$
$$- \sum_{n=1}^{N_T} \eta_n\xi_n^r - \sum_{n=1}^{N_T} \hat{\eta}_n\hat{\xi}_n^r - \sum_{n=1}^{N_T} \lambda_n\xi_n^i - \sum_{n=1}^{N_T} \hat{\lambda}_n\hat{\xi}_n^i$$
$$(9)$$

where a_n, $\hat{a}_n$, b_n, $\hat{b}_n$, η_n, $\hat{\eta}_n$, λ_n, and $\hat{\lambda}_n$ are Lagrangian multipliers.

(8) and (9) are real-valued functions defined on complex variables. The constructed Lagrange function has a saddle point which minimizes over the primal variables and maximizes over the dual variables. In order to exploit the Karush-Kuhn-Tucker (KKT) theorem, the Wirtinger's calculus [20], [26] is carried out for the complex variable $\boldsymbol{\omega}$. Besides, the gradients of real variables are computed in the traditional way. Then,

we deduce:

$$\begin{cases} \frac{\partial L_{pd}}{\partial \boldsymbol{\omega}^*} = \frac{1}{2}\boldsymbol{\omega} - \frac{1}{2}\sum_{n=1}^{N_T}((a_n - \hat{a}_n) + i(b_n - \hat{b}_n))\mathbf{x}_n = 0 \\ \frac{\partial L_{pd}}{\partial \xi_n^r} = C - a_n - \eta_n = 0, n = 1,\ldots,N_T \\ \frac{\partial L_{pd}}{\partial \hat{\xi}_n^r} = C - \hat{a}_n - \hat{\eta}_n = 0, n = 1,\ldots,N_T \\ \frac{\partial L_{pd}}{\partial \xi_n^i} = C - b_n - \lambda_n = 0, n = 1,\ldots,N_T \\ \frac{\partial L_{pd}}{\partial \hat{\xi}_n^i} = C - \hat{b}_n - \hat{\lambda}_n = 0, n = 1,\ldots,N_T. \end{cases}$$
$$(10)$$

Substituting (10) into (9), we have the following maximization task:

$$\max_{\boldsymbol{a},\hat{\boldsymbol{a}},\boldsymbol{b},\hat{\boldsymbol{b}}} -\frac{1}{2}\begin{bmatrix} \boldsymbol{a} - \hat{\boldsymbol{a}} \\ \boldsymbol{b} - \hat{\boldsymbol{b}} \end{bmatrix}^T \begin{bmatrix} Re(\mathbf{XX}^H) & -Im(\mathbf{XX}^H) \\ Im(\mathbf{XX}^H) & Re(\mathbf{XX}^H) \end{bmatrix} \begin{bmatrix} \boldsymbol{a} - \hat{\boldsymbol{a}} \\ \boldsymbol{b} - \hat{\boldsymbol{b}} \end{bmatrix}$$
$$- \epsilon\mathbf{1}^T(\boldsymbol{a} + \hat{\boldsymbol{a}} + \boldsymbol{b} + \hat{\boldsymbol{b}})$$
$$+ Re(\mathbf{y}^T)(\boldsymbol{a} - \hat{\boldsymbol{a}}) + Im(\mathbf{y}^T)(\boldsymbol{b} - \hat{\boldsymbol{b}})$$
$$\text{s. t.} \quad 0 \leqslant a_n, \hat{\alpha}_n, b_n, \hat{b}_n \leqslant C, \quad n = 1,\ldots,N_T$$
$$(11)$$

where $\mathbf{1}$ is a all-one column vector with N_T elements, $\boldsymbol{a} = [a_1,\ldots,a_{N_T}]^T$, $\hat{\boldsymbol{a}} = [\hat{a}_1,\ldots,\hat{a}_{N_T}]^T$, $\boldsymbol{b} = [b_1,\ldots,b_{N_T}]^T$, and $\hat{\boldsymbol{b}} = [\hat{b}_1,\ldots,\hat{b}_{N_T}]^T$.

In (11), the quadratic optimization function will reach its maximum with respect to the Lagrange coefficient vectors $\boldsymbol{a},\hat{\boldsymbol{a}},\boldsymbol{b},\hat{\boldsymbol{b}}$, which can be computed using quadratic programming solvers. Then, the weight $\boldsymbol{\omega}$ can be obtained according to (10), $\boldsymbol{\omega} = \sum_{n=1}^{N_T}((a_n - \hat{a}_n) + i(b_n - \hat{b}_n))\mathbf{x}_n$. In the calculation, a small identity term $\gamma\mathbf{I}$ is added in the cost function in case of ill-conditional inaccuracies [30]. Compared with the standard FBLP, the combined FBLP-SVR needs extra computation. However, the number of snapshots in the considered situations being small, the increase of computational burden is insignificant. Qualitative evaluations will be shown in the simulation part.

IV. SIMULATION RESULTS

A. Simulation Settings

In order to evaluate the performance of the proposed FBLP-SVR method, three simulations are carried out in this section. The frequency range of the step frequency radar is $1.0 - 4.0$ GHz, with $M = 21$ frequency samples. The underground structure is assumed to have three layers, as shown in Fig. 1. The medium is composed of three layers, Layer 1, Layer 2, and Layer 3. The relative permittivities and thicknesses of the layers are listed in Table I. In the simulation, four echoes (S_0, S_1, S_{M1}, and S_2) are considered. S_0, S_1, and S_2 are the primary echoes, with the corresponding time-delays $[\tau_0, \tau_1, \tau_2]$ = [6.67, 6.95, 7.89] ns. S_{M1} is the multiple echo within the first layer with time-delay $\tau_{M1} = 7.24$ ns. The time resolution is determined by $B\Delta\tau$, where B is the bandwidth and $\Delta\tau$ the time shift between two echoes [2]. If the product $B\Delta\tau$ is greater than 1, the echoes are distinguishable by conventional FFT based methods. In this simulation, the first three echoes (the first and second primary echo, the multiple echo) are overlapped. The third primary echo is not overlapped with the others. The four echoes are coherent. SNR is defined as the ratio between the power of the last primary echo and the noise variance.
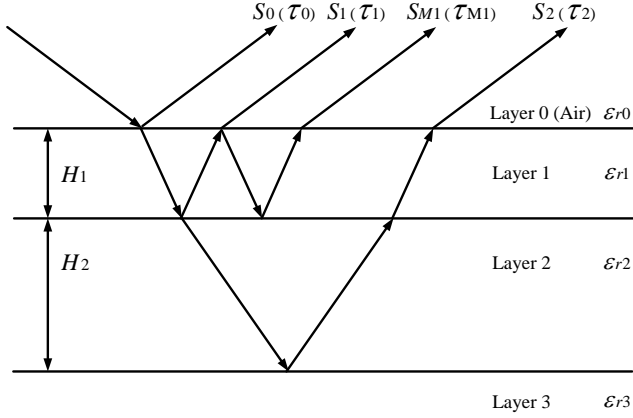
Fig. 1. Stratified layers from a simulated setup. H_i and ϵ_{ri} are the thickness and relative permittivity of Layer i ($i \in [0, 1, 2, 3]$), respectively. S_i and τ_i are the reflected echo and time-delay from interface i, respectively. S_{M1} and τ_{M1} are for the multiple echo within the first layer.

The work in [28] indicates that the smaller the order of prediction filter P is, the worse the estimation performance of LP will be. Therefore, the order P in this section is set to 19. In this situation, there should be at least 5 snapshots when using the standard FBLP so that the covariance matrix is reversible. In contrast, SVR based method does not require such constraint.

In all simulations, the SVR-related parameters are set as $\epsilon = 0$, $C = 1$, and $\gamma = 10^{-6}$. In our extensive simulation experiences, the value C and γ are insensitive parameters while ϵ should be small values. There may be other analytic parameter selection methods or other pairs of parameter settings, but the proposed FBLP-SVR shows its robustness with $\epsilon = 0$, $C = 1$ and $\gamma = 10^{-6}$ at different scenarios, as in [19].

TABLE I
VALUES OF RELATIVE PERMITTIVITY AND THICKNESS IN THE
HORIZONTAL STRATIFIED MEDIUM

$\{\epsilon_{r0}, \epsilon_{r1}, \epsilon_{r2}, \epsilon_{r3}\}$	$\{1, 3, 8, 9\}$
$\{H_1, H_2\}$ mm	$\{25, 50\}$

B. Power Spectrum Density

In the first simulation, the normalized PSD of the proposed FBLP-SVR is compared with the standard FBLP and MUSIC. We assume that the top four highest peak locations in the spectrum allow estimating the four time-delays. The simulation is conducted with 5 and 100 snapshots to show the influence of the number of snapshots on the estimation performance. SNR = 20 dB. The results are depicted in Fig. 2. The vertical dashed lines are located at the true values of time-delays. In the scenario with 5 snapshots, the proposed FBLP-SVR can detect the three primary echoes, but the amplitude of PSD of the multiple echo is very weak. The PSD of the standard FBLP has false peaks and it can not correctly detect the multiple echo. When there are 100 snapshots, FBLP and
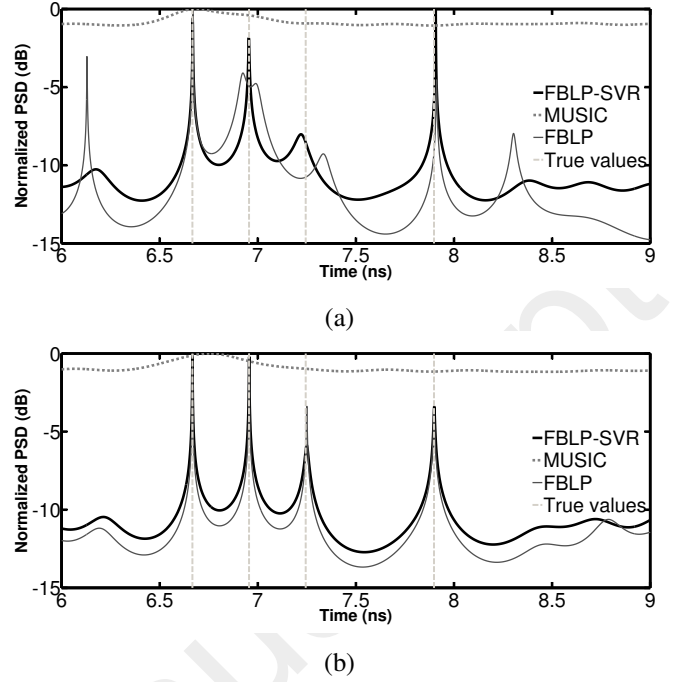

(a)

(b)

Fig. 2. PSD of FBLP-SVR, FBLP and MUSIC in the estimation of time-delays with (a) 5 snapshots and (b) 100 snapshots.

FBLP-SVR perform similarly. Both of them are capable of detecting the three primary echoes and the multiple echo. The performance of FBLP and FBLP-SVR is enhanced with more snapshots. Unfortunately, MUSIC fails to detect the echoes not only with 5 snapshots but also with 100 snapshots, due to the fact that the echoes are totally correlated.

In Fig. 2, the multiple echo has little impact on the three primary echoes, even when the first two primary echoes are overlapped with the multiple echo. Therefore, the estimation of the multiple echo is excluded in the following.

C. Performance versus the number of snapshots

In the second simulation, we evaluate the accuracy of the proposed FBLP-SVR as a function of the snapshots number L, $L \in [1,\ldots,50]$. Since the standard FBLP requires $L \geqslant 5$, its results are shown only from 5 snapshots. SVR based FLP (FLP-SVR) is also considered in this part to make a comparison with FBLP-SVR. Other settings are the same as the first simulation. For each number of snapshots, the methods are evaluated with 500 Monte Carlo trials. The performance is assessed with relative-root-mean-square-error (RRMSE), which is defined as [5]

$$RRMSE = \frac{\sqrt{\frac{1}{J}\sum_{j=1}^{J}(\hat{z}_j - z)^2}}{z} \quad (12)$$

where $\hat{z}_j$ denotes the estimated time-delay for the jth run; z is the true value; J is the number of Monte Carlo trials.

The RRMSEs of the three methods versus the number of snapshots are illustrated in Figs. 3-5. With the increasing of the number of snapshots, the RRMSEs of FBLP, FBLP-SVR and FLP-SVR decrease. FBLP-SVR has lower RRMSEs than
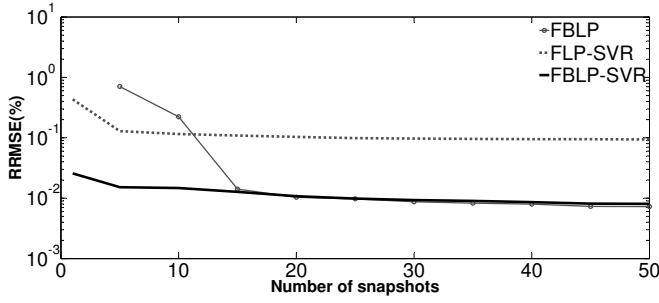
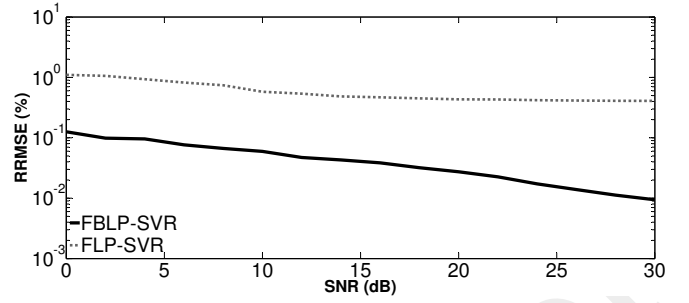Fig. 3. RRMSEs of TDE versus the number of snapshots, first primary echo.
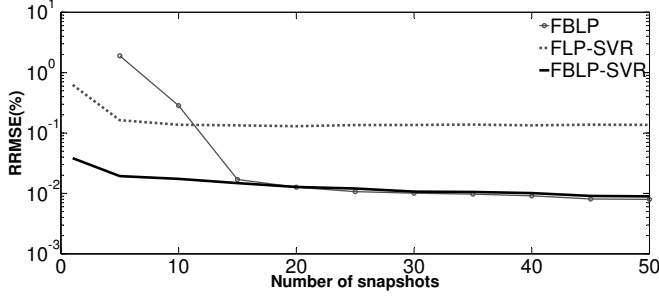

Fig. 4. RRMSEs of TDE versus the number of snapshots, second primary echo.
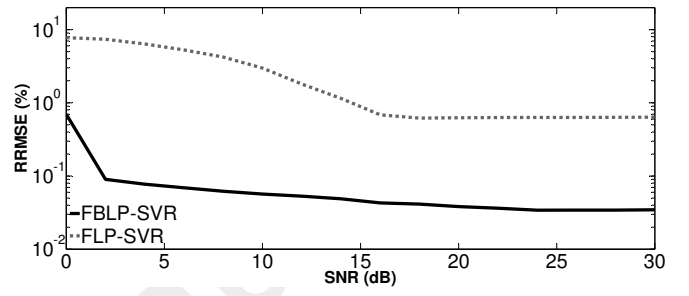
FLP-SVR at different numbers of snapshots. When the number of snapshots is large (more than 15 in this case), FBLP and FBLP-SVR achieve similar results. But when the number of snapshots is limited, the proposed FBLP-SVR has the best accuracy and outperforms the one-directional FLP-SVR and traditional FBLP.

The execution time, by a computer equipped with a processor unit (CPU) of 2.7 GHz and 16 GB of RAM, is used to get a rough idea about the computational burden of the proposed method. In the comparison, three methods (the traditional FBLP, FLP-SVR, and FBLP-SVR) are evaluated with $L = 5$ during 500 Monte Carlo trials. The average execution time of one trial using the traditional FBLP, FLP-SVR, and FBLP-SVR are 0.0674 s, 0.0816 s, and 0.0899 s, respectively. In view of the average execution time, these three methods are not time consuming. The combination of FBLP (or FLP) with SVR slightly increases the computational complexity. However, the proposed FBLP-SVR greatly improves the estimation

Fig. 5. RRMSEs of TDE versus the number of snapshots, third primary echo.

Fig. 6. RRMSEs of TDE versus SNR, first primary echo.

Fig. 7. RRMSEs of TDE versus SNR, second primary echo.

performance.

D. Performance versus SNR

In the third simulation, the methods are applied to GPR data with different SNRs ranging from 0 dB to 30 dB. Only one snapshot is considered in this simulation. The standard FBLP can not work with single snapshot hence it is not presented in the comparison. The performance of FBLP-SVR and FLP-SVR is tested with a Monte Carlo process, which consists of 500 independent runs of the methods. Figs. 6-8 show the RRMSEs of the three primary echoes using FBLP-SVR and FLP-SVR as a function of SNR. It can be seen that the RRMSEs of the three primary echoes continuously decrease as SNR increases. The estimation results of FBLP-SVR have lower RRMSEs than those of FLP-SVR. The RRMSE of the methods depends on the echo amplitude, that is, the larger the echo amplitude is, the smaller RRMSE will be. The RRMSE difference between FBLP-SVR and FLP-SVR is the smallest for the third primary echo (in Figs. 5 and 8), which might lie in the fact that the third echo is not overlapped with the other echoes.
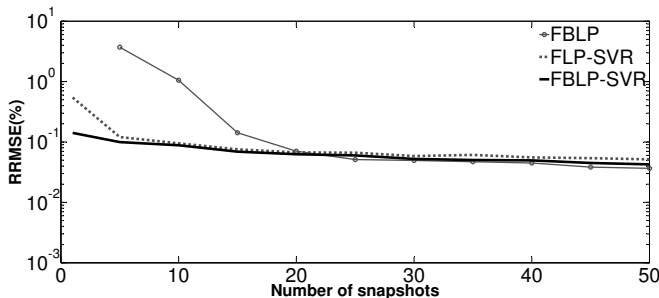
V. EXPERIMENT

In this section, the proposed method is tested with two experimental databases.

A. Laboratory experiment

In the first experiment, a PVC slab is probed in laboratory by a monostatic step frequency radar within frequency bandwidth $f \in [1.6, 3]$ GHz in far-field, with $M = 71$ frequency samples. The height of the antenna is 70 cm. The
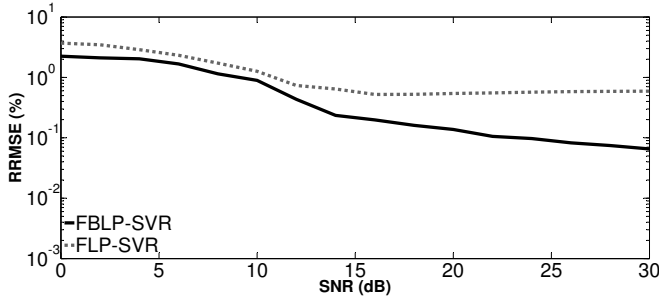
Fig. 8. RRMSEs of TDE versus SNR, third primary echo.

PVC slab has a thickness of 4 cm and relative permittivity $\epsilon_r = 2.97 + 0.015j$. In this case, the product $B\Delta\tau$ is about 0.64. Thus, the two backscattered echoes overlap with each other. The radar pulse is measured with a metal plane [2]. The data are acquired with single snapshot. The measured GPR data are preprocessed with temporal filtering and data whitening, like in [2], [5]. After that, the proposed FBLP-SVR and FBLP are applied to TDE. The order of prediction filter P is set to 70. Fig. 9 illustrates the obtained results. The backscattered echoes are overlapped and correlated with each other and there is only one snapshot. The proposed FBLP-SVR can still accurately detect the two echoes while FBLP fails because of the limitation on the number of snapshots ($L \geqslant P/[2(M - P)] = 35$). The relative error of FBLP-SVR in Fig. 9(c) is about 2.7%.

B. Field experiment

Secondly, an experiment is conducted to probe a pavement of IFSTTAR fatigue carousel [31]. The pavement consists of two layers of asphalt. The relative permittivities of the two layers are very close. The thickness of the first layer is about 5 cm. The measurement is implemented by a quasi-monostatic step frequency radar with transmitter (Tx) and receiver (Rx) close to each other. The distance between Tx and Rx antennas is constant during the B-scan. The B-scan is composed of 21 traces (A-scans). During the measurement, the far-field condition is verified. Preprocessing techniques (filtering the air wave, data whitening) are performed before applying the proposed algorithm [2], [5]. By the inverse Fourier transform, we have the B-scan obtained from the experimental data without air wave with a large frequency band ($f \in [0.8, 10.8]$ GHz), shown in Fig. 10. There are two echoes and the time shift $\Delta\tau$ between them is about 1.07 ns. Fig. 11 shows the B-scan obtained by the proposed FBLP-SVR using only one snapshot. As expected, the two echoes are well resolved by FBLP-SVR over 21 A-scans. The frequency band used in the estimation is $f \in [3.77, 4.42]$ GHz with 27 frequency elements. The prediction order P is set to 25. Thus, the product $B\Delta\tau$ is about 0.7, which means that the two echoes are overlapped. The standard FBLP can not work since the limitation on the number of snapshots is $L \geqslant 7$ and there is only one snapshot in the experiment. Fig. 12 illustrates the results obtained by the proposed method and FBLP at the 5th trace of the B-scan (5th A-scan of Fig. 10). The proposed
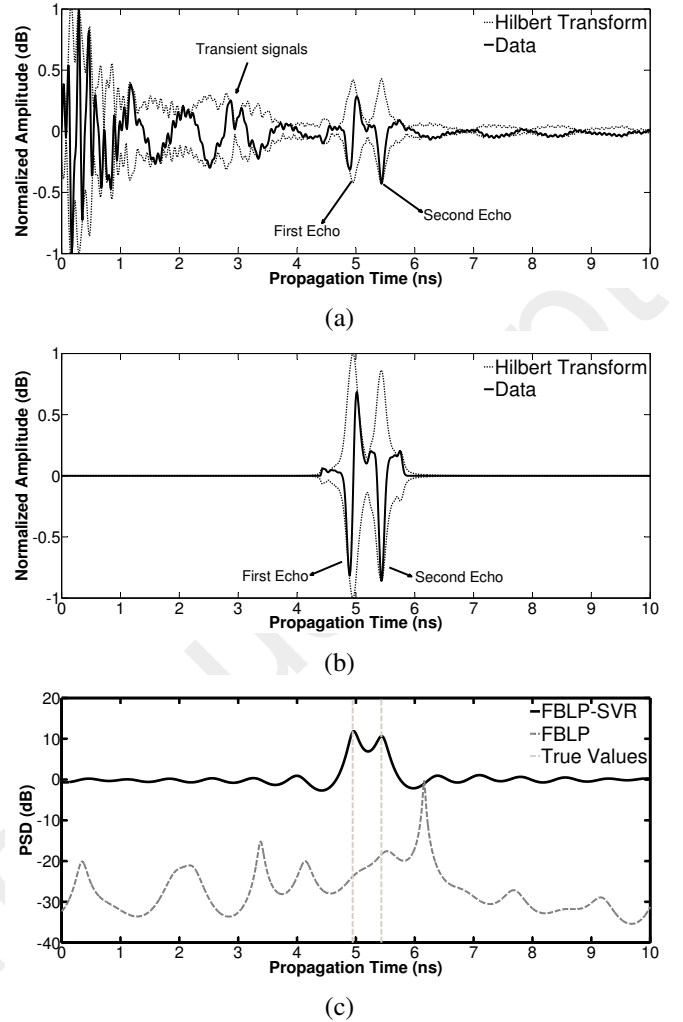

(a)

(b)

(c)

Fig. 9. Processing of GPR measurements. (a) Raw data. (b) Time-filtered data. (c) PSD of FBLP-SVR and FBLP ($B\Delta\tau \approx 0.64$).
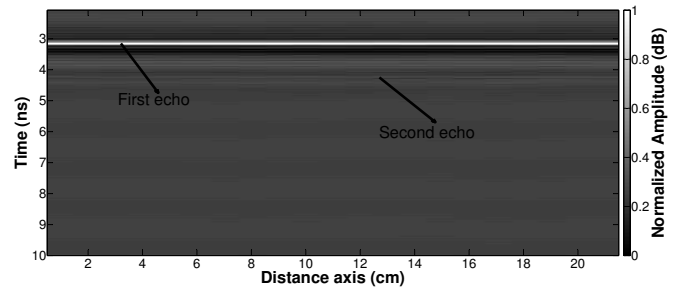

Fig. 10. Raw GPR data, B-scan with a large frequency band ($f \in [0.8, 10.8]$ GHz).

method is able to detect the two echoes as in shown Figs. 11 and 12. But FBLP shows no peak at the position of true values. In addition, the time-delays between the two echoes for the 21 A-scan are calculated. The mean and median of the estimated time shifts are 1.058 ns and 1.110 ns, respectively. The estimated time-delays are close to the real values.
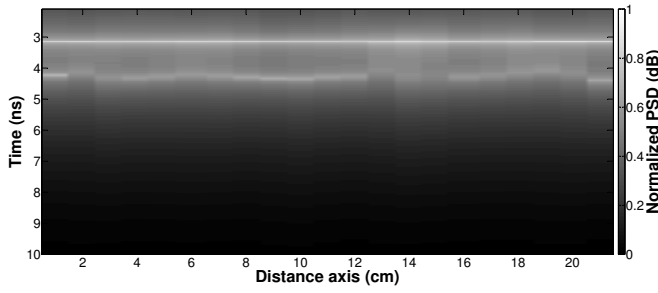
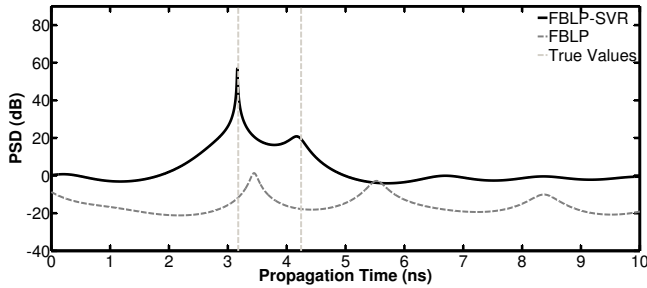Fig. 11. Estimations using FBLP-SVR, B-scan, $f \in [3.77, 4.42]$ GHz.

Fig. 12. PSD of FBLP and FBLP-SVR at the 5th A-scan.

VI. CONCLUSION

In this paper, a SVR based FBLP is proposed. The proposed method takes advantage of the good properties of FBLP and SVR. FBLP has high resolution and can decorrelate coherent signals directly. SVR is robust with small samples. The performance of the performed method is validated with numerical and experimental data, in coherent scenarios with both overlapping and non-overlapping signals and limited snapshots. The proposed FBLP-SVR outperforms the traditional FBLP and FLP-SVR methods, especially when the number of snapshots is low. Furthermore, FBLP-SVR is applicable with only one snapshot.

ACKNOWLEDGMENT

REFERENCES

[1] D. J. Daniels, *Ground penetrating radar*. 2nd ed. London, U.K.: IEE, 2004. Iet, 2004.

[2] C. Le Bastard, V. Baltazart, Y. Wang, and J. Saillard, "Thin-pavement thickness estimation using GPR with high-resolution and superresolution methods," *IEEE Trans. Geosci. Remote Sens.*, vol. 45, no. 8, pp. 2511–2519, 2007.

[3] A. Benedetto, L. Pajewski, *Civil engineering applications of ground penetrating radar*. New York, NY, USA: Springer, 2015.

[4] J. Li, C. Le Bastard, Y. Wang, G. Wei, B. Ma, and M. Sun, "Enhanced GPR signal for layered media time-delay estimation in low-SNR scenario," *IEEE Geosci. Remote Sens. Lett.*, vol. 13, no. 3, pp. 299–303, 2016.

[5] M. Sun, C. Le Bastard, Y. Wang, and N. Pinel, "Time-delay estimation using ESPRIT with extended improved spatial smoothing techniques for radar signals," *IEEE Geosci. Remote Sens. Lett.*, vol. 13, no. 1, pp. 73–77, 2016.

[6] I. Giannakis, A. Giannopoulos, and C. Warren, "A realistic FDTD numerical modeling framework of ground penetrating radar for landmine detection," *IEEE J. Sel. Topics Appl. Earth Observ. Remote Sens.*, vol. 9, no. 1, pp. 37–51, 2016.

[7] C. C. Gaudes, I. Santamaria, J. Via, E. M. Gómez, and T. S. Paules, "Robust array beamforming with sidelobe control using support vector machines," *IEEE Trans. Signal Process.*, vol. 55, no. 2, pp. 574–584, 2007.

[8] P. van Genderen and I. Nicolaescu, "Imaging of stepped frequency continuous wave GPR data using the Yule-Walker parametric method," in *Proc. Radar Conf. EURAD,* 2005, pp. 77–80, 2005.

[9] J. Xin and A. Sane, "Linear prediction approach to direction estimation of cyclostationary signals in multipath environment," *IEEE Trans. Signal Process.*, vol. 49, no. 4, pp. 710–720, 2001.

[10] T.-J. Shan, M. Wax, and T. Kailath, "On spatial smoothing for direction-of-arrival estimation of coherent signals," *IEEE Trans. Acoust., Speech, Signal Process.*, vol. 33, no. 4, pp. 806–811, 1985.

[11] L. Qu, Q. Sun, T. Yang, L. Zhang, and Y. Sun, "Time-delay estimation for ground penetrating radar using ESPRIT with improved spatial smoothing technique," *IEEE Geosci. Remote Sens. Lett.*, vol. 11, no. 8, pp. 1315–1319, 2014.

[12] R. O. Schmidt, "Multiple emitter location and signal parameter estimation," *IEEE Trans. Antennas Propag.*, vol. 34, no. 3, pp. 276–280, 1986.

[13] R. Roy and T. Kailath, "ESPRIT-estimation of signal parameters via rotational invariance techniques," *IEEE Trans. Acoust., Speech, Signal Process.*, vol. 37, no. 7, pp. 984–995, 1989.

[14] K. Ho and P. D. Gader, "A linear prediction land mine detection algorithm for hand held ground penetrating radar," *IEEE Trans. Geosci. Remote Sens.*, vol. 40, no. 6, pp. 1374–1384, 2002.

[15] A. B. Yoldemir and M. Sezgin, "Adaptive linear prediction based buried object detection with varying detector height," in *Proc. XIII Int. Conf. Ground Penetrating Radar*, pp. 1-4, 2010.

[16] C. R. Ratto, K. D. Morton, L. M. Collins, and P. A. Torrione, "Analysis of linear prediction for soil characterization in GPR data for countermine applications," *Sensing and Imaging*, vol. 15, no. 1, pp.1–20, 2014.

[17] C. Ratto, P. Torrione, and L. Collins, "Estimation of soil permittivity through autoregressive modeling of time-domain ground-penetrating radar data," in *Proc. IEEE Int. Conf. Wireless Information Technology and Systems (ICWITS)*, pp. 1–4, 2010.

[18] V. N. Vapnik, *Statistical learning theory. Adaptive and learning systems for signal processing, communications and control*. New York: Wiley, 1998.

[19] A. El Gonnouni, M. Martinez-Ramon, J. L. Rojo-Álvarez, G. Camps-Valls, A. R. Figueiras-Vidal, and C. G. Christodoulou, "A support vector machine MUSIC algorithm," *IEEE Trans. Antennas Propag.*, vol. 60, no. 10, pp. 4901–4910, 2012.

[20] P. Bouboulis, S. Theodoridis, C. Mavroforakis, and L. Evaggelatou-Dalla, "Complex support vector machines for regression and quaternary classification," *IEEE Trans. Neural Netw. Learn. Syst.*, vol. 26, no. 6, pp. 1260–1274, 2015.

[21] N. Xu, *Applications of support vector machines in electromagnetic problems*. PhD thesis, 2011.

[22] J. L. Rojo-Álvarez, G. Camps-Valls, M. Martínez-Ramón, E. Soria-Olivas, Á. Navia-Vázquez, and A. R. Figueiras-Vidal, "Support vector machines framework for linear signal processing," *Signal Process.*, vol. 85, no. 12, pp. 2316–2326, 2005.

[23] J. L. Rojo-Álvarez, M. Martínez-Ramón, M. de Prado-Cumplido, A. Artés-Rodríguez, and A. R. Figueiras-Vidal, "Support vector method for robust ARMA system identification," *IEEE Trans. Signal Process.*, vol. 52, no. 1, pp. 155–164, 2004.

[24] S. S. Haykin, *Adaptive filter theory*, 3rd ed. Englewood Cliffs, NJ: Prentice- Hall, 1996.

[25] Y.-H. Chen and C.-T. Chiang, "Kalman-based spatial domain forward-backward linear predictor for DOA estimation," *IEEE Trans. Aerosp. Electron. Syst.*, vol. 31, no. 1, pp. 474–479, 1995.

[26] P. Bouboulis and S. Theodoridis, "Extension of Wirtinger's calculus to reproducing kernel Hilbert spaces and the complex kernel LMS," *IEEE Trans. Signal Process.*, vol. 59, no. 3, pp. 964–978, 2011.

[27] J. Li and R. Wu, "An efficient algorithm for time delay estimation," *IEEE Trans. Signal Process.*, vol. 46, no. 8, pp. 2231–2235, 1998.

[28] Y. L. Wang, H. Chen, Y. Peng, and Q. Wan, *Spatial spectrum estimation theory and algorithm*. Beijing: Tsinghua University, 2004.

[29] D. W. Tufts and R. Kumaresan, "Estimation of frequencies of multiple sinusoids: Making linear prediction perform like maximum likelihood," *Proc. IEEE*, vol. 70, no. 9, pp. 975–989, 1982.

[30] M. Martínez-Ramón and C. Christodoulou, "Support vector machines for antenna array processing and electromagnetics," *Synthesis Lectures on Computational Electromagnetics*, vol. 1, no. 1, pp. 1–120, 2005.

[31] J. M. Simonin, V. Baltazart, C. Le Bastard, and X. Dérobert, "Progress in monitoring the debonding within pavement structures during accelerated pavement testing on the fatigue carousel," in *MCD2016, 8th International conference on Mechanisms of Cracking and Debonding in Pavements*, pp. 749-755, 2016.